TÜBİTAK

Turkish Journal of Chemistry

http://journals.tubitak.gov.tr/chem/

Research Article

Turk J Chem
(2020) 44: 833 – 840
© TÜBİTAK
doi:10.3906/kim-2003-16

Isothermal compressibility and isobaric thermal shrinkage of a porous α-alumina compact: thermodynamic calculations

Yüksel SARIKAYA[1], **Müşerref ÖNAL**[1,*], **Abdullah Devrim PEKDEMIR**[2]
[1]Department of Chemistry, Faculty of Science, Ankara University, Ankara, Turkey
[2]Graduate School of Natural and Applied Sciences, Ankara University, Ankara, Turkey

Received: 09.03.2020 • **Accepted/Published Online:** 10.05.2020 • **Final Version:** 01.06.2020

Abstract: Two methods were proposed to calculate the thermodynamic parameters of porous ceramic compacts depending on their molar volume change with applied pressure and heating temperature, respectively. Molar volume of the porous α-alumina (α-Al_2O_3) compact was evaluated according to literature depending on both the applied pressure at room temperature and the heating temperature at atmospheric pressure. The isothermal compressibility coefficient, Gibbs energy, and work done on the compact by compression were calculated. The thermal shrinkage coefficient and activation energy as well as the change in enthalpy, entropy and Gibbs energy were calculated for partial sintering. The spontaneous nature of the treatments were discussed with respect to the obtained results.

Key words: Activation energy, α-alumina, compressibility, shrinkage, thermodynamics

1. Introduction

Several low temperature phases of aluminum oxide convert to α-alumina (α-Al_2O_3) through heating over 1150 °C [1,2]. Its natural form is known as the corundum mineral. Because of its high mechanical, thermal, and chemical stability porous α-alumina ceramics have been used in different areas such as catalyst support, membrane, electrode and thermal insulator. [3–5]. The void volume in a compact solids with widths smaller than 2 nm, between 2–50 nm and larger than 50 nm are called micropore, mesopore, and macropore, respectively [6,7].

The change in the relative volume of a porous compact with increasing pressure at constant temperature is defined as the isothermal compressibility [8–10]. Similarly, change in the relative volume of a porous compact with increasing heating temperature at constant pressure is defined as the isobaric thermal shrinkage [11,12].

The driving force for shrinkage is the chemical potential (molar Gibbs energy) difference of the mobile chemical species between the active center on the surface of the meso- and micropores in the compact [13,14]. Shrinkage occurs via the transfer of these species from higher to lower chemical potentials through several mechanisms such as grain boundary, surface and volume diffusions as well as evaporation and condensation [15–17].

There are numerous experimental results found in the literature for the kinetics and thermodynamics of isothermal compressibility [18–20], thermal shrinkage [21–23], and sintering [24–27]. Although there have been several mathematical modelling or computer simulations attempts, there are no studies concentrated on

*Correspondence: onal@science.ankara.edu.tr

numerical calculations using basic thermodynamic relations. So, the aim of the present study is to calculate the change in some thermodynamic quantities during the isothermal compressibility and isobaric thermal shrinkage of a porous α-Al_2O_3 compact using the data evaluated from literature.

2. Materials and methods

The molar volume of the calcined porous α-Al_2O_3 compact was derived from literature depending on the applied pressure at constant temperature, as well as the heating temperature at constant pressure [6]. In addition, the isothermal compressibility and thermal shrinkage coefficients, together with the change in some thermodynamic quantities such as work, enthalpy, entropy and Gibbs energy were calculated, respectively. All results were given in SI units.

3. Results and discussion

3.1. Isothermal compressibility

The molar volume (V) of the cylindrical porous α-Al_2O_3 compacts calcined at 1200 °C for 2 h were calculated using their diameter and thickness taken from the literature data depending on the applied pressure (p) ranging from 140 to 2080 bar (Table 1). The plot of V against p shows a decreasing curve in Figure 1. This change is due to the reduction of macropores to mesopores through application of extremely high pressing pressure on the compact at constant temperature whereas the meso- and micropores remain unchanged. The isothermal compressibility coefficient (κ) can be derived from the power equation of this curve given below;

$$V = 6 \times 10^{-4} / p^{0,138} \tag{1}$$

$$\kappa = -\frac{1}{V}\left(\frac{\partial \mathrm{V}}{\partial p}\right)_T = \frac{0,138}{p} \tag{2}$$

where the negative sign has been incorporated into the definition so that κ is positive. The κ values produce a linear change with $1/p$ calculated for each pressure (Table 1).

Table 1. Pressing pressure (p), molar volume (V) and isothermal compressibility (κ) for a porous α-Al_2O_3 compact after calcination at 1200 °C for 2 h.

p / 10^8 Pa	0.140	0.350	0.555	0.970	2.080
V / 10^{-5} m^3 mol^{-1}	6.390	5.671	5.205	4.781	4.451
κ / 10^{-9} Pa^{-1}	9.857	3.943	2.486	1.423	0.663

The Gibbs energy (ΔG) for the isothermal compression was calculated between the pressures $p_1 = 1.40 \times 10^7$ Pa and $p_2 = 20.80 \times 10^7$ Pa from the well-known basic thermodynamic relation:

$$\left(\frac{\partial G}{\partial p}\right)_T = V \tag{3}$$

$$\Delta G = \int_{p_1}^{p_2} V dp \tag{4}$$

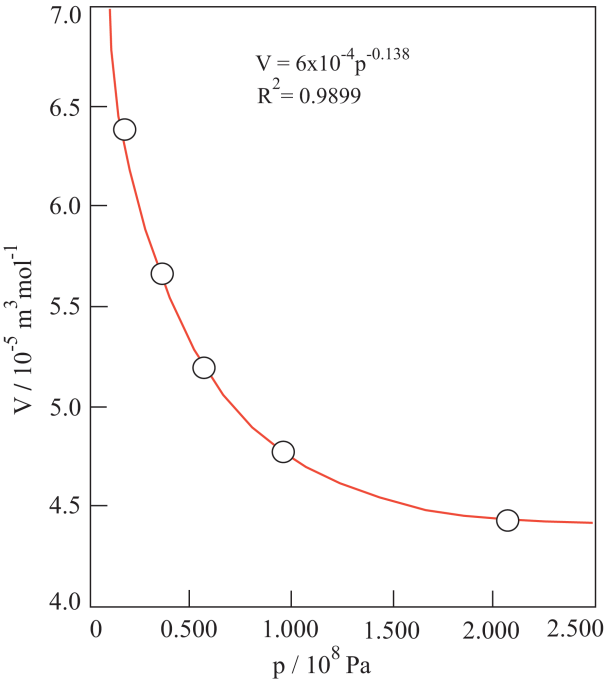

Figure 1. Variation in molar volume of α-Al_2O_3 compact with applied pressure.

$$\Delta G = \int_{p_1}^{p_2} (6 \times 10^{-4} / p^{0.138})\, dp = 9293\, J\, mol^{-1} \tag{5}$$

The positive value of ΔG is due to the unspontaneous nature of the compression.

It has been internationally accepted that the work done on a system is positive and from the system is negative. Mechanical work done on the compact during the compression process has been calculated using the $d(pV) = pdV + Vdp$ relationship in the following form;

$$\delta w = -pdV = -d(pV) + Vdp \tag{6}$$

$$w = -\int_{V_1}^{V_2} pdV = -\int_{p_1V_1}^{p_2V_2} d(pV) + \int_{p1}^{p_2} Vdp \tag{7}$$

$$= -p_2V_2 + p_1V_1 + \Delta G \tag{8}$$

$$= (-2080 \times 4.451 + 140 \times 6.39)\, J\, mol^{-1} + 9293\, J\, mol^{-1} = 930\, J\, mol^{-1}$$

where the unit for pressure and volume is N/m^2 and m^3/mol, respectively. The inequality of $\Delta G \neq w$ indicates irreversibility of isothermal compression according to the second law of thermodynamics.

3.2. Thermal shrinkage

Molar volume (V) of the cylindrical porous α-Al_2O_3 compacts compressed at 280 bar was calculated using the diameter and thickness taken from literature data, for temperatures (T) in the range of 1150–1550 °C (Table

2). The plot of V against T reveals a decreasing curve in Figure 2. This change originates from the reduction of mesopores to micropores, followed by the closing of these micropores with increasing heating temperature at constant pressure. On the other hand, the macropores remain almost unchanged. The polynomial equation of this curve was evaluated as given below:

$$V = -9 \times 10^{-11} T^2 + 2 \times 10^{-7} T - 10^{-4} \tag{9}$$

where T is the absolute temperature.

Table 2. Heating temperature (T), molar volume (V) and thermal shrinkage (α) for a porous α-Al_2O_3 compact.

t / °C	1150	1250	1350	1450	1550
T / K	1423	1523	1623	1723	1823
V / 10^{-5} m^3 mol^{-1}	6.00	5.69	5.41	4.79	4.04
$-(\partial V_T/\partial T)_p$ / 10^{-8} m^3 mol^{-1} K^{-1}	5.614	7.414	9.214	11.014	12.814
α / 10^{-4} K^{-1}	9.36	13.03	17.03	22.99	31.72
-ln α	6.974	6.643	6.375	6.075	5.754
T^{-1} / 10^{-4} K^{-1}	7.027	6.566	6.161	5.804	5.485

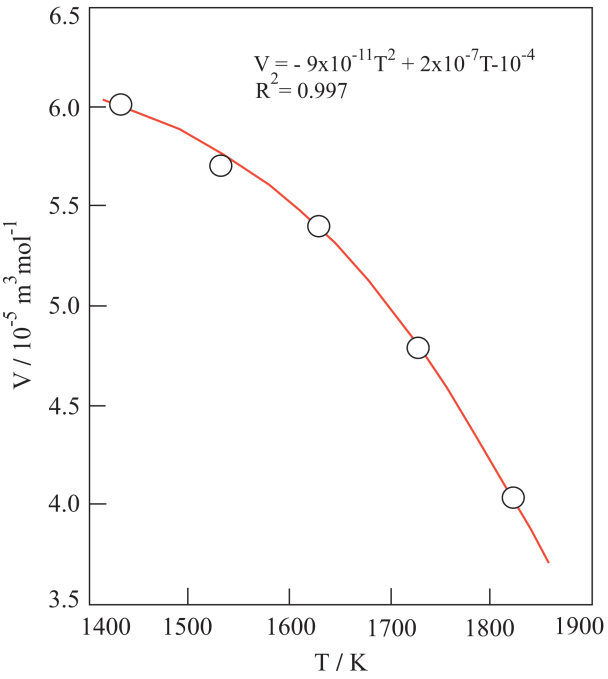

Figure 2. Variation in molar volume of α-Al_2O_3 compact with absolute sintering temperature.

The thermal shrinkage coefficient (α) was calculated for each temperature using the following definition;

$$\alpha = -\frac{1}{V}\left(\frac{\partial V}{\partial T}\right)_p \tag{10}$$

and given in Table 2. The curvilinear change of α versus T is depicted in Figure 3.

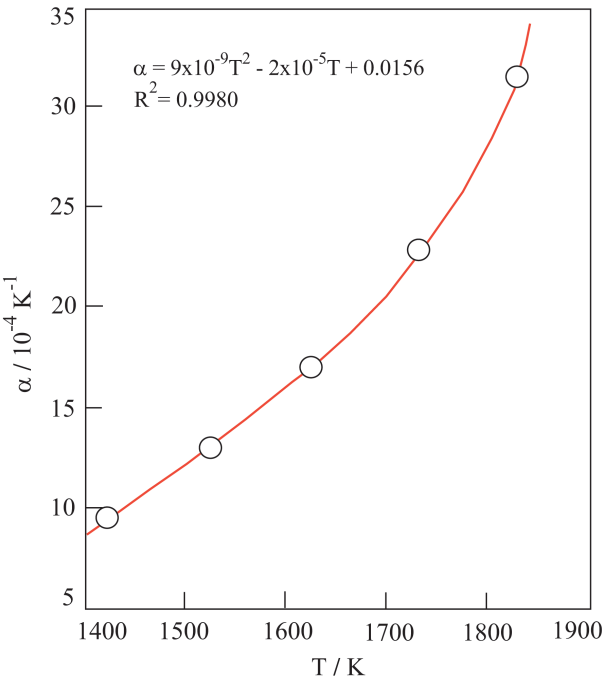

Figure 3. Variation in thermal shrinkage coefficient with absolute sintering temperature.

Since the plot of $ln\ \alpha$ against $1/T$ shows a linear relationship as seen in Figure 4, α behaves like a reaction rate constant and obeys the well-known Arrhenius equation;

$$ln\alpha\ =\ ln\,A - \frac{\mathrm{E}^{\#}}{\mathrm{RT}} \tag{11}$$

where A is the preexponential factor, $E^{\#}$ is the activation energy, R is the universal gas constant, and T is the absolute temperature. The Arrhenius relation for thermal shrinkage was evaluated according to equation of the linear change shown in Figure 4:

$$\ln\alpha\ = -\,17582 - \frac{7364.6}{\mathrm{T}} \tag{12}$$

By comparison of the last two relations, the apparent activation energy for the thermal shrinkage can be calculated as follows:

$$E^{\#}\ =\ (slope)\,R\,(13) \tag{13}$$

$$E^{\#}\ =\ (7364.6K)\times(8.314\,J\,K^{-1}\,mol^{-1})\ =61229\,J\,mol^{-1}$$

The enthalpy and entropy changes (ΔH and ΔS) of the α-Al_2O_3 compacts during shrinkage between the temperatures $T_1\ =\ 1423$ K and $T_2\ =\ 1823$ K were calculated using the basic thermodynamic relations as given below:

$$(\partial\mathrm{H}/\partial\mathrm{T})_{\mathrm{p}}=\mathrm{C_p} \tag{14}$$

$$\Delta\mathrm{H}=\int_{\mathrm{T_1}}^{\mathrm{T_2}}\mathrm{C_p}\mathrm{dT}=\mathrm{C_p}(\mathrm{T_2}-\mathrm{T_1}) \tag{15}$$

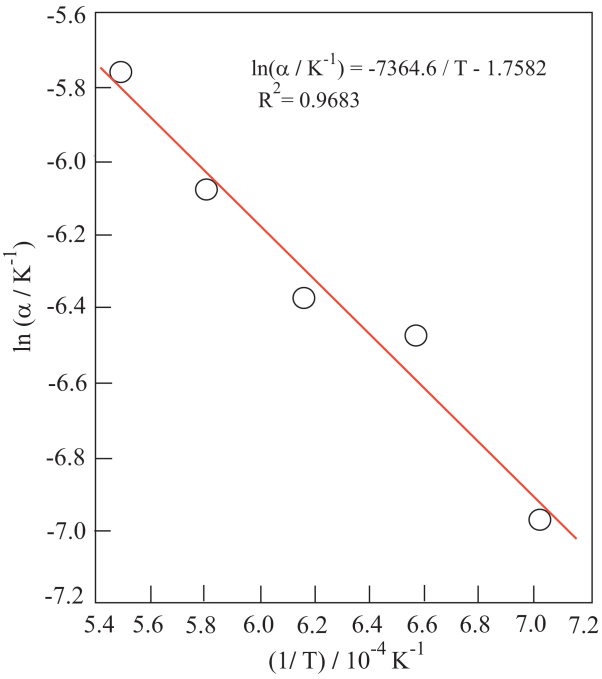

Figure 4. Arrhenius plot for the thermal shrinkage.

$$\Delta H = (79.04\, J\, K^{-1}\, mol^{-1}) \times (1823 - 1423)\, K = 31616\, J\, mol^{-1}$$

and

$$(\partial \mathrm{S}/\partial \mathrm{T})_{\mathrm{p}} = \mathrm{C_p}/\mathrm{T} \tag{16}$$

$$\Delta \mathrm{S} = \int_{\mathrm{T_1}}^{\mathrm{T_2}} \frac{\mathrm{C_p}}{\mathrm{T}}\, \mathrm{dT} = \mathrm{C_p} \ln \frac{\mathrm{T_2}}{\mathrm{T_1}} \tag{17}$$

$$\Delta S = (79.04\, J\, K^{-1}\, mol^{-1}) \ln \frac{1823}{1423} = 19.6\, JK^{-1}\, mol^{-1}$$

where $\mathrm{C}_p\,(79.04\ \mathrm{J\ K^{-1}\ mol^{-1}})$ is the temperature independent heat capacity of the α-$\mathrm{Al_2O_3}$ [28]. The positive values originate from the increasing enthalpy and entropy of the compacts by during the thermal shrinkage. The inequality of $\Delta H < E^{\#}$ shows the endothermic nature of thermal shrinkage which is partly sintering.

The temperature dependency of the Gibbs energy (ΔG) was also calculated using the last two results in via the basic thermodynamic relation given below:

$$\Delta G = \Delta H - T\Delta S \tag{18}$$

$$\Delta G = 31616 - 19.6T \tag{19}$$

Since thermodynamic equilibrium is established at $\Delta G = 0$, the equilibrium temperature can be obtained as follows:

$$T = \Delta H/\Delta S \tag{20}$$

$$T = 31616\,J\,mol^{-1}/19.6\,J\,K^{-1}\,mol^{-1} = 1613\,K\,(1340C)$$

Therefore, the value of ΔG is positive before 1340 °C and negative afterwards. The case where $\Delta G>0$ that reveals thermal shrinkage is an unspontaneous process. It is spontaneous when $\Delta G<0$. Finally, temperature dependency of the equilibrium constant (K) for the partly sinterization of the porous α-alumina compact can evaluate using the van't Hoff equation.

$$\ln \mathrm{K} = -\frac{\Delta \mathrm{G}}{\mathrm{RT}} = -\frac{31616 + 19.6\mathrm{T}}{\mathrm{RT}} = -\frac{3803}{\mathrm{T}} + 19.6 \tag{21}$$

4. Conclusion

Some thermodynamic interpretations have proposed on the isothermal compressibility and isobaric thermal shrinkage of a porous ceramic compact. Change in the molar volume of a porous solid compact with pressure at constant temperature and with the temperature at constant pressure has been experimentally determined. Isothermal compressibility and thermal shrinkage of the compact were theoretically examined using the corresponding molar volume change with the basic kinetic and thermodynamic relationships. The unspontaneous nature and irreversibility of these processes were also discussed depending on the result of the thermodynamic calculations. The activation energy for the partial sintering of the porous compacts during thermal shrinkage was determined using the thermal shrinkage coefficient in the Arrhenius equation. In addition, sintering stages can distinguish from each other depending on different activation energies.

Acknowledgments

We are grateful to the Ankara University Research Fund (Project No: 16L0430013) for financial support for this study.

References

1. Ada K, Sarıkaya Y, Alemdaroğlu T, Önal M. Thermal behaviour of alumina precursor obtained by the aluminium sulphate-urea reaction in boiling aqueous solution. Ceramics International 2003; 29: 513-518.
2. Ahmad J, Tariq MI, Ahmad R, Mujtaba-ul-Hassan S, Mehmood M et al. Formation of porous α-alumina from ammonium aluminum carbonate hydroxide whiskers. Ceramics International 2019; 45: 4645-4652.
3. Hirata Y, Takehara K, Shimonosono T. Analyses of Young's modulus and thermal expansion coefficient of sintered porous alumina compacts. Ceramics International 2017; 43: 12321-12327.
4. Li H, Wen W, Chang C. Facile fabrication of surfactant-templated silica membrane on porous alumina support. Materials Letters 2017; 192: 60-63.
5. Zhang M, Chang Y, Bermejo R, Jiang G, Sun Y et al. Improved fracture behavior and mechanical properties of alumina textured ceramics. Materials Letters 2018; 221: 252-255.
6. Hugo P, Koch H. Production of porous alumina with defined bimodal pore structure. German Chemical Engineering 1979; 2: 24-30.
7. Gawel B, Øye G. Hierarchical γ-alumina monoliths with macro- and meso porosity prepared by using cross-linked dextran gel beads as the template. Materials Letters 2013; 95: 86-88.
8. Frey RG, Halloran JW. Compaction behavior of spray-dried alumina. Journal of the American Ceramic Society 1984; 67: 199-203.
9. Widodo RT, Hassan A. Compression and mechanical properties of directly compressible pregelatinized sago starches. Powder Technology 2015; 269: 15-21.

10. Katz JM, Buckner IS. Full out-of-die compressibility and compactibility profiles from two tablets. Journal of Pharmaceutical Sciences 2017; 106: 843-849.
11. Chaim R, Levin M, Shlayer A, Estournes C. Sintering and densification of nanocrystalline ceramic oxide powders: a review. Advances in Applied Ceramics 2008; 107: 159-169.
12. Muto D, Hashimoto S, Honda S, Daiko Y, Iwamoto Y. Characterization of porous alumina bodies fabricated by high-temperature evaporation of boric acid with sodium impurity. Ceramics International 2018; 44: 3678-3683.
13. Thümmler F, Thomma W. The sintering process. Metallurgical Reviews 1967; 12: 69-108.
14. Burnham AK. An nth-order Gaussian energy distribution model for sintering. Chemical Engineering Journal 2005; 108: 47-50.
15. Pines ML, Bruck HA. Pressureless sintering of particle-reinforced metal-ceramic composites for functionally graded materials: Part II. Sintering model. Acta Materialia 2006; 54: 1467-1474.
16. Hirata Y, Shimonosono T, Sameshimo T, Sameshima S. Compressive mechanical properties of porous alumina powder compacts. Ceramics International 2014; 40: 2315-2322.
17. Hirata Y, Shimonosono T. Theoritical prediction of compressive strength, Young's modulus and strain at fracture of sintered porous alumina compacts. Ceramics International 2016; 42: 3014-3018.
18. Caligaris RE, Topolevsky R, Maggi P, Brog F. Compaction behaviour of ceramic powder. Powder Technology 1985; 42: 263-267.
19. De Oliveira GLP, Ceria MAR, Missagia RM, Archilla NL, Figuiredo L et al. Pore volume compressibilites of sandstones and carbonates from helium porosimetry measurements. Journal of Petroleum Science Engineering 2016; 137: 185-201.
20. Ghyngazov SA, Frangulyan TS. Impact of pressure in static and dynamic pressing of zirconia ultradisperse powders on compact density and compaction efficiency during sintering. Ceramics International 2017; 43: 16555-16559.
21. Bailliez S, Nzihou A. The kinetics of surface area reduction during isothermal sintering of hydroxyapatite adsorbent. Chemical Engineering Journal 2004; 98: 141-152.
22. Ada K, Önal M, Sarıkaya Y. Investigation of the intra-particle sintering kinetics of mainly agglomerated alumina powder by using surface area reduction. Powder Technology 2006; 168: 37-41.
23. Kutty MG, Bhaduri SB, Zhou H, Yaghoubi A. In situ measurements of shrinkage and temperature profile in microwave- and conventionally-sintered hydroxyapatite bioceramic. Materials Letters 2015; 161: 375-378.
24. Sarıkaya Y, Ada K, Önal M. A model for initial-stage sintering thermodynamics of an alumina powder. Powder Technology 2008; 188: 9-12.
25. Hirata Y, Hara A, Aksay IA. Thermodynamic of densification of powder compact. Ceramics International 2009; 35: 2667-2674.
26. Sarıkaya Y, Önal M. An indirect model for sintering thermodynamics. Turkish Journal of Chemistry 2016; 40: 841-845.
27. Mane RB, Panigrahi BB. Effect of alloying order on non-isothermal sintering kinetics of mechanically alloyed high entropy alloy powders. Materials Letters 2018; 217: 131-134.
28. Alberty RA, Silbey RJ. Physical Chemistry . New York, NY, USA: John Wiley and Sons, 1992.